American Mineralogist, Volume 73, pages 798–808, 1988

Effects of compositional variation on the crystal structures of pyroxmangite and rhodonite

LINDA R. PINCKNEY
Corning Glass Works, Sullivan Park FR-51, Corning, New York 14831, U.S.A.
CHARLES W. BURNHAM
Department of Earth and Planetary Sciences, Harvard University, Cambridge, Massachusetts 02138, U.S.A.

ABSTRACT

As adjacent members of the pyroxene-pyroxenoid polysomatic series, constructed of fragments of the wollastonite (W) and pyroxene (P) structures, pyroxmangite (WPP) and rhodonite (WP) possess very similar structures with comparable site distortions and cation ordering patterns. The two structures respond quite similarly to cation substitutions. Octahedral and tetrahedral distortions generally lessen and the silicate chains straighten as larger cations substitute for smaller. Both structures exhibit limited stepwise ordering of cations over the octahedral sites, with large cations preferentially entering the sites on the edges of the octahedral bands. Detailed structural responses to cation substitution generally parallel those observed in pyroxenes.

The characteristics of the inner octahedral sites strongly influence several structural parameters, including the sizes and configurations of the outer polyhedra. There is, however, no well-defined mean cation size limit that differentiates rhodonite from pyroxmangite from pyroxene. Structural parameters for both rhodonite and pyroxmangite structures change smoothly with composition and produce only minor structural adjustments. These adjustments, however, produce localized higher-energy structural configurations that cluster at the boundaries between the W and P modules of the structures. Such configurations include a strongly kinked tetrahedral chain, short Si-Si distances, and a highly distorted octahedron. In contrast, the P-P boundary in pyroxmangite is virtually distortion-free. Concentrations of strain energy at W-P boundaries likely play a major role in controlling phase transformations in this system.

INTRODUCTION

Pyroxenes and anhydrous pyroxenoids have the general chemical formula $MSiO_3$, where M most commonly is Ca, Mg, Fe, and Mn. Their structures consist of single chains of silicate tetrahedra arranged in layers parallel to (100) that alternate with layers containing bands of divalent cation octahedra; oxygen atoms are approximately closest packed (Prewitt and Peacor, 1964). The various structures differ in the periodicity of the tetrahedral chain and in the corresponding arrangement of the octahedrally coordinated cations. In this manner they constitute a structural series that has been classified according to the number n of tetrahedra between offsets that interrupt pyroxene-like chain configurations (Liebau, 1962). Pyroxene represents one end member of this structural series: a pyroxenoid with no offsets ($n = \infty$).

When the entire structural configuration of octahedral bands and tetrahedral chains is considered, these structures are seen to constitute a polysomatic series, which is defined as a group of distinct structures constructed of different numbers of slablike portions of end-member structures—in this case, of wollastonite and clinopyroxene. All members of the pyroxenoid series may be constructed by appropriately stacking these wollastonite (W) and pyroxene (P) modules, thereby deriving wollastonite (W), rhodonite (WP), pyroxmangite (WPP), ferrosilite III (WPPP), and pyroxene (P). The structures of rhodonite ($n = 5$) and pyroxmangite ($n = 7$) are illustrated in Figure 1. Bustamite, another three-repeat pyroxenoid, is based on a different linkage of octahedral and tetrahedral layers and therefore is not a member of this series. This concept is discussed more fully by Koto et al. (1976) and by Thompson (1978).

A number of workers have addressed the observed temperature, pressure, and compositional stability limits that exist for each pyroxenoid structure (e.g., Akimoto and Syono, 1972; Ito, 1972; Maresch and Mottana, 1976; Ohashi and Finger, 1978; Brown et al., 1980). Akimoto and Syono (1972) determined that a pyroxenoid of $MnSiO_3$ composition undergoes successive polymorphic transformations from rhodonite to pyroxmangite to clinopyroxene and ultimately to garnet-type structures as pressure increases at constant temperature. A similar trend is observed with respect to composition: As mean cation size decreases, structures with increasing n predominate.

These observations raise an intriguing question: Can

0003–004X/88/0708–0798$02.00

TABLE 1. Crystal-structure refinements of pyroxmangite and rhodonite

Symbol	Composition	Sample source	Reference
		Pyroxmangites	
CWB-P	$(Fe_{0.83}Ca_{0.13}Mn_{0.02}Mg_{0.02})SiO_3$	Apollo 11 site*	Burnham (1971)
Roth-P	$(Mn_{0.15}Mg_{0.85})SiO_3$	Synthetic**	D. Rothbard (unpub.)
FH-P	$(Mn_{0.51}Mg_{0.49})SiO_3$	Synthetic**	Finger and Hazen (1978)
OF-P	$(Mn_{0.82}Fe_{0.07}Mg_{0.09}Ca_{0.02})SiO_3$	Japan†	Ohashi and Finger (1975)
Aj-P	$(Mn_{0.97}Mg_{0.02}Ca_{0.01})SiO_3$	Japan††	Pinckney and Burnham (1988)
Nar-P	$MnSiO_3$	Synthetic‡	Narita et al. (1977)
		Rhodonites	
FH-R	$(Mn_{0.62}Mg_{0.38})SiO_3$	Synthetic**	Finger and Hazen (1978)
MT-R	$(Mn_{0.685}Mg_{0.315})SiO_3$	Synthetic**	Murakami and Takéuchi (1979)
Peac-R	$(Mn_{0.75}Mg_{0.15}Ca_{0.10})SiO_3$	Balmat, NY§	Peacor et al. (1978)
OF-R	$(Mn_{0.81}Fe_{0.07}Mg_{0.06}Ca_{0.05})SiO_3$	Japan†	Ohashi and Finger (1975)
Nar-R	$MnSiO_3$	Synthetic‡	Narita et al. (1977)

* Lunar microgabbro.
** Synthesized by J. Ito.
† Taguchi mine: regionally metamorphosed manganese ore deposit.
†† Ajiro mine: mineralized manganese ore lens in chert.
‡ Synthesized by Akimoto and Syono (1972).
§ Metamorphosed sedimentary evaporite sequence.

the phase relationships be readily understood in terms of structural attributes identifiable in each phase? The stability of micas, for example, is related to the geometric fit of the octahedral and tetrahedral sheets (Hazen and Wones, 1972, 1978); if the octahedral layer becomes so large that normal tetrahedral rotations and polyhedral distortions can no longer compensate for it, then the sheet silicate will be rendered less stable relative to alternative structures. We might anticipate that there could be similar constraints inherent in the linkages of the octahedral bands and tetrahedral chains of pyroxenoids.

Previous work

Although the chemical and structural relations among the pyroxenes have been studied intensively (e.g., Cameron and Papike, 1981), analogous studies for the pyroxenoids are relatively scarce. Ohashi and Finger (1975) compared the structures of pyroxmangite and rhodonite and noted the close topologic and configurational correspondence between certain cation polyhedra in the two structures. Ohashi and Finger (1978) studied the role of the octahedral cations in the crystal chemistry of the three–tetrahedral repeat hydrous and anhydrous pyroxenoids and demonstrated that the different stacking configurations of tetrahedral and octahedral layers determine the resulting cation-ordering patterns and limit the extent of solid solution.

Very little has been written, however, concerning the relationship between bulk composition and structural stability of the intermediate pyroxenoids. Liebau (1962) noted that the chain configuration in pyroxenoids is apparently a function of the average size of the octahedrally coordinated cations. More specifically, based on the observation (e.g., Freed and Peacor, 1967) that pyroxene stability depends on the relative size of the M1 octahedron, Takéuchi (1977) suggested that the sizes of the cations in the inner M1-like octahedra of pyroxenoids are primarily responsible for their relative stabilities. Although this correlation was briefly examined by Murakami and Takéuchi (1979), the exact nature of the relationship has not been defined. Nor has there been any systematic study, similar to the pyroxene studies of Ohashi et al. (1975) and Ribbe and Prunier (1977), regarding the specific effects of compositional variation, temperature, or pressure on these crystal structures.

This paper examines the effects of compositional variation on the crystal structures of pyroxmangite and rhodonite, concentrating primarily on Mn-Mg substitutions. Because there is substantial compositional overlap between the Mn-Mg pyroxmangite and rhodonite stability fields along the $MgSiO_3$-$MnSiO_3$ join, these compositions are particularly suitable for examining any developing structural instabilities. Accordingly, data from previous crystal-structure refinements of pyroxmangite and rho-

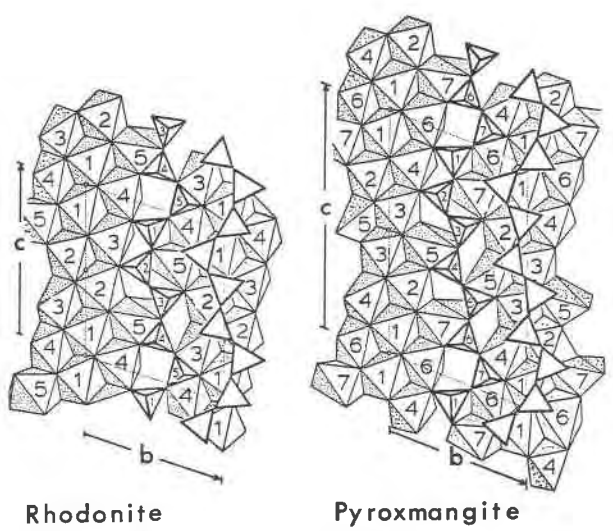

Fig. 1. Projections of the rhodonite and pyroxmangite structures onto (100). Octahedral (M) sites in both structures are identified by number. After Ohashi and Finger (1975).

donite (listed in Table 1) have been assessed along with those from a new refinement of a nearly pure $MnSiO_3$ pyroxmangite. Data for pyroxferroite (Burnham, 1971) are also included in the analysis.

We employ the $C\bar{1}$ setting for the pyrxoxenoids; data taken from previous refinements based on the $P\bar{1}$ setting have been converted into their $C\bar{1}$ equivalents. The series of Appendix Tables A1 through A5 compiles selected data for pyroxmangite and rhodonite taken or calculated from the crystal-structure refinements listed in Table 1.

Structural variations

Cell expansion

For the most part, the pyroxmangite and rhodonite structures respond very similarly to compositional variation. Cell parameters of both structures, for example, increase fairly smoothly with the substitution of Mn for Mg, although small amounts of Ca present in natural rhodonites cause marked increases in the a and b cell dimensions.

A complete description of lattice strain due to chemical substitution of a larger cation (Ca or Mn) for a smaller one (Mg) requires that a strain ellipsoid be calculated (Ohashi and Burnham, 1973). Using the cell parameters given in Appendix Table A1 and the computer program STRAIN, written by Y. Ohashi, the magnitudes and orientations of strain ellipsoids for several compositional increments of pyroxmangite and rhodonite were calculated. Because of the relative complexity and lower symmetry of these structures, their ellipsoids are somewhat more difficult to interpret than are those of pyroxenes. Nevertheless, several clear trends emerge. The pyroxmangites, whose compositions range from $(Mn_{0.15}Mg_{0.85})SiO_3$ to $MnSiO_3$, exhibit two distinct strain-ellipsoid orientations depending on Mn content. These are summarized in Table 2 as average low- and high-Mn ellipsoids, with the breaking point at about $Mn_{50}Mg_{50}$. The orientation of the average strain ellipsoid for Ca-free rhodonites, which are all relatively Mn-rich, strongly resembles that of the high-Mn pyroxmangites.

TABLE 2. Principal strain components of expansion due to chemical substitution

	Principal strain components × 10^{-3} per 1% Mg → Mn	Orientation: Angle with +a	+b	+c
	Average low-Mn pyroxmangite (Mn_{15} → Mn_{51})			
ϵ_1	26(2)	131(6)	60(9)	68(9)
ϵ_2	20(1)	109(9)	146(9)	35(9)
ϵ_3	13(2)	47(6)	75(8)	64(8)
Volume	59(3)			
	Average high-Mn pyroxmangite (Mn_{51} → Mn_{97})			
ϵ_1	42(1)	87(4)	25(2)	88(2)
ϵ_2	32(1)	25(2)	76(4)	127(2)
ϵ_3	16(1)	65(2)	110(2)	37(2)
Volume	90(2)			
	Rhodonite (Ca-free, Mn_{62} → Mn_{100})			
ϵ_1	37(2)	47(15)	37(21)	119(21)
ϵ_2	34(3)	117(18)	60(27)	54(20)
ϵ_3	18(3)	55(3)	110(8)	49(3)

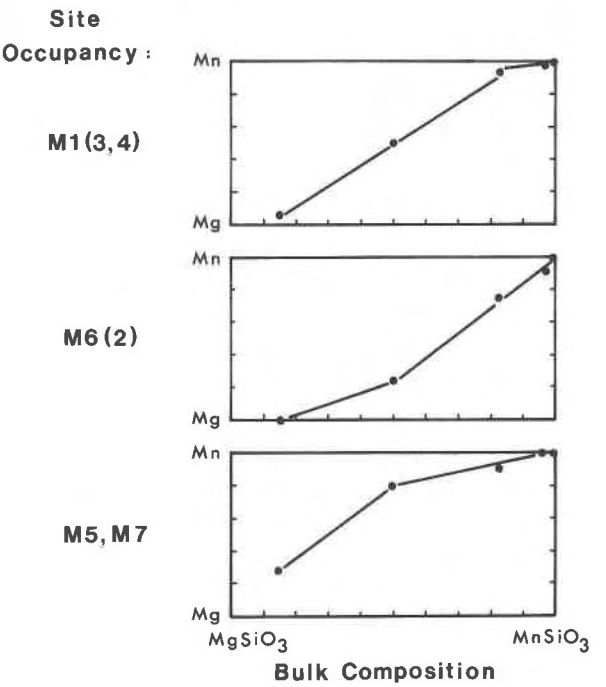

Fig. 2. Cation site occupancy, Mn/(Mn + Mg), as a function of bulk composition for pyroxmangites along the join $MgSiO_3$-$MnSiO_3$. Points represent average site occupancies over the two or three sites indicated.

The reason for this change in ellipsoid magnitude and orientation becomes clear if we examine cation ordering patterns. Figure 2 plots M-site occupancies in pyroxmangite as a function of bulk composition $(Mn,Mg)SiO_3$; three ordering patterns are apparent. Although cation occupancies of the M1, M3, and M4 sites vary linearly with bulk composition, the other sites display a limited stepwise ordering pattern, with the M2 and M6 sites showing a marked preference for small cations and the large, seven-coordinated M5 and M7 polyhedra taking up Mn early in the series.

Addition of Mn to a low-Mn pyroxmangite produces a strain ellipsoid in which the greatest expansions lie close to the b-c plane, with the largest expansion about halfway between the b and c axes. This reflects a marked expansion of the structure along directions in which the density of M5–O and M7–O bonds is highest. The relatively small volume expansion, compared with that of the equivalent composition increment $(Mn_{0.51}Mg_{0.49})SiO_3$-$(Mn_{0.97}$ "Mg"$_{0.03})SiO_3$, is due to the ability of the M5 and M7 polyhedra, located at the edges of the octahedral band, to expand into the adjacent void space without unduly distorting the structure.

As Mn content increases, expansion of the small and inner octahedra begins to contribute most to the overall expansion. The resulting strain ellipsoid suggests a less

distorted expansion or "swelling" of the octahedral band due to the more isotropic expansion of the inner octahedra, with the greatest expansions perpendicular to the band and the least expansion parallel to the band because of the constraints imposed by the tetrahedral chain. At this stage, the direction of greatest expansion lies parallel to the "dense zone" of cations, first described for pyroxenes by Morimoto et al. (1966) and defined for pyroxmangites and rhodonites by Aikawa (1979). In pyroxmangite, the dense zone is parallel to $[031]_{C\bar{1}}$, which for the Ajiro sample is oriented 90°, 30°, and 79° from the *a*, *b*, and *c* axes, respectively. The direction of largest expansion is thus parallel to the zone having densest concentration of M and Si cations.

Silicate chain

Chemical substitutions in the octahedral sites necessarily influence the silicate chains as well since they link the octahedral bands. The chains respond to their new environment with expansion and distortion of individual tetrahedra and by rotation of tetrahedra with respect to each other. Because the number of crystallographically distinct tetrahedra is fairly large, there are many degrees of freedom in the chains; thus substantial structural compensations can be achieved with only small adjustments in each parameter.

Individual tetrahedra. Mean Si–O bond lengths do not change appreciably (<0.006 Å) with the substitution of Mn for Mg (App. Table A2). As in almost all single-chain silicates, the Si–OC (bridging oxygen) bonds are longer than the nonbridging bonds, and of the latter, the Si–OA (apical oxygen) bonds are longer than the Si–OB bonds.

In both pyroxmangite and rhodonite, tetrahedral distortions decrease as mean octahedral cation size increases (App. Table A4). This effect is seen also in pyroxenes (Cameron and Papike, 1981) and is due to the disproportionate lengthening of the OC-OC edge of the tetrahedron, which opens up the OC–Si–OC angle and thereby lessens the distortion. This is a simple yet effective means of stretching the chain without increasing the average Si–O distance. Tetrahedral distortions are roughly the same for pyroxmangite and rhodonite of similar compositions (App. Table A4); they increase along the chain from Si1 to Si7, primarily because the Si4 through Si7 tetrahedra share edges with octahedra. The distortions of the non–edge-sharing tetrahedra are comparable to those in clinopyroxene (e.g., Ohashi, et al., 1975).

Tetrahedral chain angles. As the mean octahedral-cation radius increases, the tetrahedral chain undergoes an overall gradual straightening by about 2° (see App. Table A5). Not unexpectedly, the "straightest" chain angles (OC-OC-OC closest to 180°) are those associated with the P modules. The most highly kinked angle is OC5-OC6-OC7 in pyroxmangite, and its rhodonite equivalent is OC3-OC4-OC5. This angle is associated with the tetrahedral "triplet" of the W module and is located at the boundary between the W and P modules. Although the angle widens by up to 6° as Mn replaces Mg, it remains significantly more kinked in pyroxmangite than in rhodonite of identical composition. This suggests that the W-P boundary—and, as will be demonstrated, the W module itself—becomes less favorable energetically in pyroxenoids with smaller mean cation size.

The Si-Si distances within the chains range from 2.94 to 3.11 Å. The longer Si-Si distances are those associated with the P modules. The shorter ones are the Si6-Si7 distances in pyroxmangite and the equivalent Si4-Si5 distances in rhodonite, as well as the Si1-Si2 distances in both structures. Both of these distances are located at the W-P module interface. The former is a result of the highly kinked chain angle mentioned above. The latter is the shortest Si-Si distance in each of these pyroxenoids and is a manifestation of the inherent peculiarity of the pyroxenoid tetrahedral chain as it jogs sideways to follow the octahedral band, causing two tetrahedra (Si1 and Si2) to point in the same direction. Oxygens OB1 and OB2 thus lie on the same side of the "backbone" of the chain formed by the bridging oxygens. This is the natural consequence of connecting a W and a P module.

Octahedral band

The octahedral bands in chain silicates contain two basically different kinds of sites, those on the inside of the bands and those on their edges. The inner octahedra possess edges defined by the apical oxygens of the tetrahedral chain. Except for the M1 octahedra in pyroxenoids, these octahedra are situated in the P modules, have environments very similar to that of M1 in pyroxene, and, like the pyroxene M1 octahedron, are relatively undistorted. The M1 octahedra of pyroxmangite and rhodonite, which possess three such "apical edges" because of the lateral jog of the tetrahedral chains across them, are the basis of the W module and as such have no pyroxene equivalents. The sites on the edges of the bands are distorted polyhedra that share edges with tetrahedra and correspond to the M2 polyhedra in pyroxenes.

In light of these correspondences, Takéuchi (1977) proposed the designation of M1*i* for the inner octahedra (including M1) and M2*j* for the outer polyhedra, where $i = 0, 1, 2, \cdots$ and $j = 1, 2, \cdots$. The M1*i* sites in pyroxmangite, for example, comprise M1 through M3. Although we retain the original nomenclature for each individual site in this paper, the concept of basically different M1*i* and M2*j* polyhedra is useful since both the geometries and the resulting cation occupancies of the two groups are quite distinct. The concept of M1-like and M2-like sites also facilitates comparison with pyroxenes.

Inner octahedra. The changes in mean M–O distance ($\overline{M\text{–}O}$) as a function of site occupancy for the inner octahedra in pyroxmangite and rhodonite are plotted in Figure 3. $M4_{pxmn}$ and $M3_{rhod}$ are included in the figure although they are not true M1*i* octahedra. Several interesting features are apparent in these plots. Whereas the $\overline{M\text{–}O}$ of several of the octahedra, such as M1 and M4 of pyroxmangite, exhibit a linear relationship with cation substitution, the curves for M2 and M3 exhibit a slight

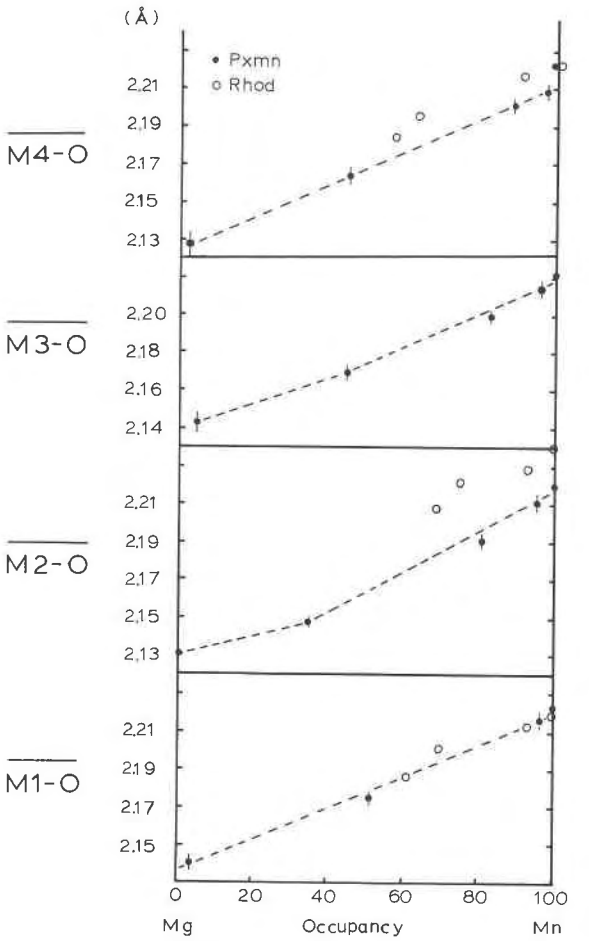

Fig. 3. Mean M–O bond distances ($\overline{M–O}$) of the regular octahedra of pyroxmangite and rhodonite as a function of site occupancy Mn/(Mn + Mg).

bend, which suggests that the oxygen framework of these polyhedra may be held open by the nature of the structure to a minimum $\overline{M–O}$ of about 2.13 Å. Moreover, for any given cation occupancy, the mean bond lengths of the rhodonite octahedra are almost always longer than those of the equivalent pyroxmangite octahedra. This effect is particularly pronounced for M2.

Distortion parameters for the inner octahedra of both pyroxmangite and rhodonite (App. Table A4) indicate that, although distortions generally are slightly greater for Mg-rich compositions, the presence of Ca in the outer polyhedra does not cause significant distortion of the inner octahedra. Distortion is comparable for topologically equivalent octahedra of the two structures except that the distortion of $M2_{rhod}$ is greater than that of $M2_{pxmn}$, particularly in angle variance. The M2 octahedra are discussed further in the next section.

Finally, it should be noted that the M3 octahedron in pyroxmangite, located at the boundary between adjacent P modules, is consistently less distorted than the otherwise similar M2 octahedron, located at the W-P boundary. This effect is observed also in the WPPP structure, ferrosilite III (Weber, 1983).

Outer octahedra. A plot of $\overline{M–O}$ for the outer sites shows considerable scatter because of the varying coordinations of these polyhedra. Whereas $M4_{pxmn}$ and $M3_{rhod}$ are fairly regular octahedra, the $M5_{pxmn,rhod}$ and $M7_{pxmn}$ sites have effective oxygen coordinations described better as seven than as six, with distortion from ideal increasing in the order $M7_{pxmn} < M5_{rhod} < M5_{pxmn}$. This distortion difference is due to a combination of polyhedral angles and to the slightly different coordination characteristics of the three polyhedra: $M5_{pxmn}$ and $M5_{rhod}$ are coordinated by four short and three medium-to-long bonds, whereas $M7_{pxmn}$ has four short, two medium, and one very long bond. By virtue of this one very long bond, $M7_{pxmn}$ is the closest to six-coordinated; in fact, its distortion parameters calculated using the six shortest bonds are similar to those of M2 in clinoferrosilite [$\langle\lambda\rangle = 1.06$, $\sigma_{\theta 2} = 164$ (Ohashi et al., 1975)].

Substitution of Mn for Mg does not cause significant distortion of the large M5 and M7 polyhedra in pyroxmangite. Addition of Ca to these sites, however, causes a considerable increase in distortion and a closer approach to seven-coordination as short M–O bonds lengthen disproportionately relative to long bonds, which undergo little or no change. The rhodonite M5 polyhedron responds to Ca occupancy in the same manner. Unlike in pyroxmangite, however, the rhodonite M5 polyhedron responds also to Mg substitution, causing the oxygen configuration to shift to four short, one medium, and two long bonds. This polyhedron, therefore, tends toward seven-coordination in Mg-rich as well as in Ca-rich rhodonites, although the geometry of the polyhedra is quite different.

The small irregular $M6_{pxmn}$ and $M4_{rhod}$ octahedra undergo significant changes in configuration as cation size increases, resulting in a coordination closer to five than to six in Mn-rich compositions. Five-coordination is particularly pronounced when Ca is present. Such seemingly anomalous behavior, in which effective coordination decreases as cation size increases, is readily understood in light of the fact that, although large cations (except Ca) do enter this site, they are filling neighboring cation positions at a much faster rate (recall Fig. 2). In pyroxmangite, this causes the tetrahedral chain angle OC5-OC6-OC7 to straighten by up to 6°, which in turn pulls the OA7 oxygen atom sharply away from the M6 cation (Fig. 4). Charge repulsion also increases the distance between the now-larger M6 cation and the Si7 cation with which the M6 cation shares a polyhedral edge. An important result of these relative movements is that, as Mn or Ca fills the M5 and M7 sites, the OA7 oxygen moves away from the M6 cation faster than the cation itself moves away from Si7. Eventually the OA7 oxygen is farther from the M6 cation than is the Si7 atom; in Ca-rich pyroxferroite, these distances are 2.902 and 2.873 Å, respectively (Burnham, 1971).

The M6 octahedron is a component of the W module

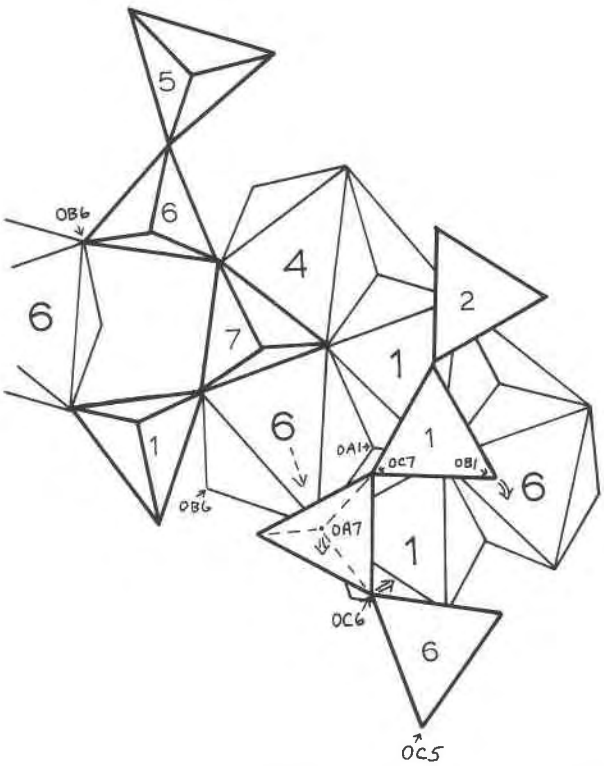

Fig. 4. Configuration changes of the M6 polyhedron in pyroxmangite as Mn/(Mn + Mg) increases. Double arrows indicate relative movements of atoms. As the tetrahedral chain angle OC5-OC6-OC7 straightens, the OA7 oxygen atom moves away from the M6 cation. The distance between the M6 cation and the Si7 atom also increases because of increased charge repulsion, but at a slower rate. Eventually, the M6 cation is closer to Si7 than it is to OA7, resulting in M6 becoming five-coordinated.

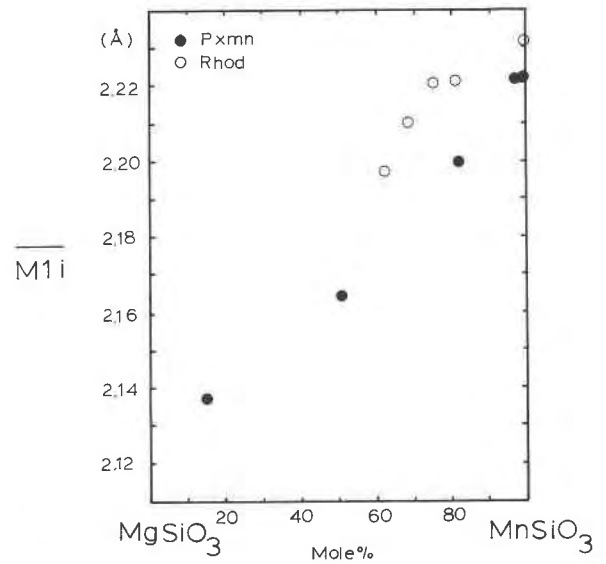

Fig. 5. Variation of grand mean M1*i*–O bond length, $\overline{M1i}$, as a function of bulk composition for Mg-Mn pyroxmangites and rhodonites.

and as such is best suited geometrically for larger cations (Ohasi and Finger, 1978). Presence of small cations in the site causes the extreme kinking of the OC5-OC6-OC7 tetrahedral chain angle (discussed above) and contributes to the "unfavorableness" of W modules in structures with small mean cation size.

Significance of the M1*i* octahedra

The pyroxene M1 octahedron does not vary drastically among the different structure types (ortho, clino, and proto); it is appropriate to consider it the major building block of the pyroxene structure (Cameron and Papike, 1981). Various workers (e.g., Ribbe and Prunier, 1977; Cameron and Papike, 1981) have demonstrated that the M1 octahedron determines to a large extent the unit-cell dimensions, the relative displacement and kinking of the tetrahedral chain, and the size and configuration of the M2 polyhedron. We therefore might anticipate that the topologically equivalent M1*i* octahedra would play an equally central role in the pyroxenoids, and indeed this is the case.

The significance of the M1*i* octahedra is most easily seen by correlating their size with other structural parameters and comparing the correlations with those observed in pyroxenes. It is convenient to define $\overline{M1i}$ for pyroxenoids as the grand mean M1*i*–O bond length, where M1*i* octahedra include M1 through M3 in pyroxmangite and M1 and M2 in rhodonite (Murakami and Takéuchi, 1979). A plot of $\overline{M1i}$ as a function of bulk composition along or near the join $MgSiO_3$-$MnSiO_3$ for pyroxmangites and rhodonites is given in Figure 5.

Unlike pyroxenes, the cell parameters of natural pyroxmangite and rhodonite follow $\overline{M1i}$ only approximately, because moderate amounts of Ca in the outer M2*j* sites exert little influence on the M1*i* ocatahedra but have a marked effect on the cell edges. In most respects, however, the relationship of $\overline{M1i}$ with other structural parameters parallels those observed in pyroxenes.

More unexpected is the influence of the M1*i* octahedra on the M2*j* polyhedra. One significant observation that has emerged from pyroxene studies is that the sizes of polyhedra are frequently constrained by the nature of the structure itself and that an important control is the M1 octahedron. Ghose and Wan (1975), for example, observed that in $MCaSi_2O_6$ clinopyroxenes (i.e., with constant M2 cation occupancy), the average M2–O distance increases linearly with increasing mean M1–O distance, which implies that the size of the outer octahedra may be ultimately controlled by the size of the inner octahedra. Figure 6 indicates that a similar relationship exists for pyroxmangite and rhodonite as well. Taking the term $\overline{M2j}$ to represent the grand mean M2*j*–O bond length for each particular structure, two curves of $\overline{M2j}$ versus $\overline{M1i}$ have been plotted for each structure, reflecting two different assignments of coordination numbers to the M2*j* polyhedra. Although the plots for pyroxmangite are very

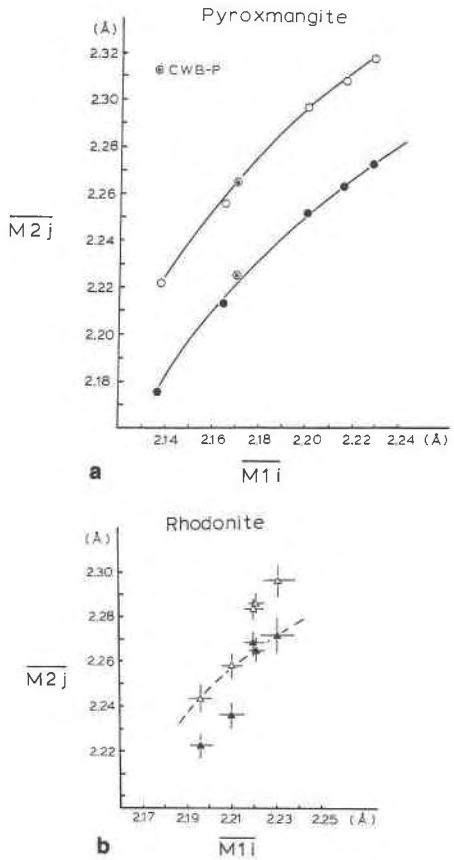

Fig. 6. Variation of grand mean bond lengths $\overline{M2j}$ with $\overline{M1i}$. (a) Pyroxmangites: the lower curve (filled circles) considers all M sites as six-coordinated except M6 in CWB-P pyroxferroite, which is taken as five-coordinated. The upper curve (open circles) considers M5 and M7 as seven-coordinated. (b) Rhodonites: filled triangles take all M sites as six-coordinated, whereas open triangles take M5 as seven-coordinated. Significance of the dashed composite curve is explained in the text.

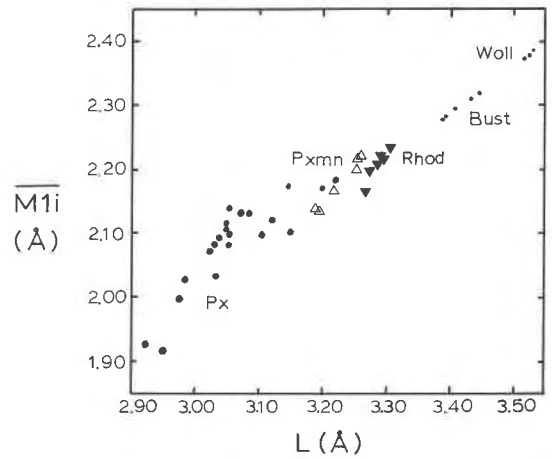

Fig. 7. Variation of grand mean bond length $\overline{M1i}$ with L parameter (see text) for pyroxmangites and rhodonites.

well defined, the rhodonite data produce breaks in both curves. These breaks are a result of the previously discussed change in $M5_{rhod}$ coordination with increasing Mg content. Because the sixth and seventh oxygen atoms are then approximately equidistant from the M5 cation, considering $M5_{rhod}$ as six-coordinated produces artificially low data points for the relatively Mg-rich rhodonites MT-R and FH-R. When M5 is taken as seven-coordinated in these Mg-rich phases, however, their distances plot on the lower curve defined by the points of the Mn-rich rhodonites (in which M5 is more nearly six-coordinated). This composite curve is given as the dashed line in Figure 6b.

The strong correlation apparent in these curves is even more remarkable given that it encompasses not only Mn ⇌ Mg substitution but also Ca-bearing compositions such as the Ca-rich pyroxferroite CWB-P. It is clear, therefore, that regardless of bulk composition, the sizes of the M2j polyhedra are linked to and constrained by the sizes of the inner octahedra.

As this correlation seems to hold true for chain silicates in general, it may be one way in which the M1i octahedra ultimately control the relative stability of the pyroxenoid structures (including pyroxenes), as suggested by Takéuchi (1977). The relationship between the M1i cations and pyroxenoid stability, however, is by no means a simple one. For example, the large degree of overlap in $\overline{M1i}$ values between pyroxmangites and rhodonites (Fig. 5), as indeed in the bulk composition itself, indicates that although a trend does exist, there certainly is no cut-off point in M1i size that controls the relative stability of pyroxmangite and rhodonite.

In an attempt to define the correlation between the M1i cations and pyroxenoid stability, Murakami and Takéuchi (1979) examined the relationship between $\overline{M1i}$ and the average distance between apical oxygens along the tetrahedral chain, which is a qualitative measure of chain extension. They defined a quantity

$$L = \left(\sum_{j=1}^{n} l_j + l_0\right)/(n+1),$$

where n is the periodicity of the tetrahedral chain and L is essentially the average distance between apical oxygens including the apical–apical distance l_0 across the triplet. They then plotted L versus $\overline{M1i}$ for a number of pyroxenoid and pyroxene structures; their plot is reproduced in Figure 7. The set of data points for each structure type defines an approximately straight line, with very little overlap in L values between structures. Murakami and Takéuchi therefore concluded that there is a critical limit of L for each structure type. They suggested that this limit in L might be related to l_0 because of the systematic change in l_0 with $\overline{M1i}$. The term l_0, however, merely reflects the distance across the relatively undistorted M1 octahedron, and there is considerable overlap in l_0 values for pyroxmangite and rhodonite (see Table 3).

We suggest instead that the lack of overlap in L values, at least between pyroxmangite and rhodonite, is due primarily to the significantly different sizes and distortions of the M2 octahedron. Although the M2 octahedron in rhodonite is topologically equivalent to that of pyroxmangite, i.e., located in the P module adjacent to the W-P boundary, it is much larger and more distorted in rhodonite than in pyroxmangite. The difference is independent of bulk composition and apparently is an inherent, structurally controlled phenomenon. The high distortion of this octahedron suggests that the P module may be less stable in rhodonite than in pyroxmangite of identical composition.

Conclusions

Rhodonite (WP) and pyroxmangite (WPP) are adjacent members of the pyroxenoid-pyroxene polysomatic series; they possess very similar structures with octahedral and tetrahedral sites that are topologically equivalent and exhibit comparable distortions and cation ordering patterns. As a result, the two structures respond in much the same way to compositional variation.

As larger cations replace smaller ones in these structures, octahedral and tetrahedral distortions generally lessen, and the silicate chains straighten. Both structures exhibit limited stepwise ordering of cations, with larger cations preferentially entering the large sites on the edges of the octahedral bands. Very large cations, such as Ca, appear restricted to these sites and so place limitations on bulk composition. Mean Si–O distances change very little. These structural responses to cation substitution mirror those observed in pyroxenes.

Also as in pyroxenes, the nature of the octahedra on the inside of the band (M1i octahedra) strongly influences the entire structure, including the ultimate size and configuration of the outer polyhedra. Although there is a general correlation between cation size and structure type, with the number of P modules per unit cell increasing with decreasing mean cation size, there is no critical cutoff in mean size that differentiates pyroxmangite from rhodonite or, for that matter, from pyroxene. Structural parameters for both pyroxenoid structures change smoothly with composition and produce only minor structural adjustments.

These adjustments, however, produce localized higher-energy structural configurations that cluster at the boundaries between the W and P modules, leaving the P-P boundaries virtually strain-free. Decreasing mean cation size in a pyroxenoid, for example, results in smaller P modules. The configurations and minimum sizes of W modules, however, are constrained by the tetrahedral chains; the chains develop strong kinks at the W-P boundaries, forcing pairs of Si cations close together to Si-Si distances significantly shorter than the 3.0 Å proposed by Hill and Gibbs (1979) as the lower limit of nonbonded Si-Si contacts. Both the W modules and the W-P boundaries therefore become energetically less stable in compositions with smaller mean cation size. It is significant that in pyroxmangite, the P modules remain relatively undistorted regardless of composition; nearly all of the distortion occurs at the W-P boundaries.

Because decreasing cation size in rhodonite leads to distortions that cause higher-energy configurations to develop at W-P boundaries, W modules are destabilized relative to P modules, and P-P boundary stability is thereby enhanced. This tends to favor nucleation of additional P modules within the mineral. A mechanism for such a nucleation process consistent with this notion has been formulated by Angel et al. (1984) and by Veblen (1985) to explain phase reactions in the pyroxene-pyroxenoid system. Conversely, as cation size increases in pyroxmangite, the W module is stabilized and W-P boundaries become more favorable.

Accumulation of higher-energy strained configurations at W-P boundaries as cation substitution proceeds suggests that a yet-unidentified maximum strain limit may contribute energetically to phase transformations in this system. Indeed, such buildup of distortion-induced strain energy at W-P interfaces can explain the common observation in transmission electron microscopy (Ried and Korekawa, 1980; Czank and Liebau, 1980; Alario Franco et al., 1980; Czank and Simons, 1983) that excess P modules, and hence excess P-P boundaries, are much more common in pyroxenoids than are excess W modules.

TABLE 3. Additional parameters for pyroxmangite and rhodonite

	$\overline{M1–O}$	$\overline{M1i}$*	$\overline{M2j}$**	$\overline{M2j}$†	ℓ_o‡	L‡
			Pyroxmangites			
Nar-R	2.223	2.222	2.272	2.318	2.635	3.263
Aj-P	2.220	2.214	2.264	2.309	3.609	3.260
OF-P	2.207	2.199	2.252	2.297	3.599	3.252
FH-P	2.174	2.164	2.213	2.256	3.515	3.218
Roth-P	2.139	2.137	2.177	2.223	3.457	3.194
CWB-P	2.185	2.169	2.226§	2.265§	3.646	3.216
			Rhodonites			
Nar-R	2.219	2.231	2.272	2.296	3.626	3.301
OF-R	2.213	2.221	2.265	2.287	3.599	3.292
Peac-R	2.219	2.220	2.269	2.284	3.569	3.293
MT-R	2.200	2.210	2.236	2.258	3.537	3.283
FH-R	2.186	2.197	2.223	2.244	3.511	3.271

* M1i comprises $M1–M3_P$. $M1–M2_R$. $\overline{M1i}$ = mean M–O bond distance of these octahedra.

** M2j comprises $M4–M7_P$. $M3–M5_R$. All polyhedra are considered to be six-coordinated.

† M2j sites are the same, only $M5_P$, $M7_P$, and $M5_R$ are considered to be seven-coordinated.

‡ ℓ_o and L are defined in the text.

§ M_e is considered to be five-coordinated.

Acknowledgments

This research was supported by National Science Foundation grant EAR-7920095 to C.W.B. We thank D. R. Peacor and R. J. Reeder for helpful reviews, through which the manuscript was substantially improved.

References cited

Aikawa, N. (1979) Oriented intergrowth of rhodonite and pyroxmangite and their transformation mechanism. Mineralogical Journal, 9, 255–269.

Akimoto, S., and Syono, Y. (1972) High pressure transformations in $MnSiO_3$. American Mineralogist, 57, 76–84.

Alario Franco, M.A., Jefferson, D.A., Pugh, N.J., Thomas, J.M., and Bishop, A.C. (1980) Lattice imaging of structural defects in a chain silicate: The pyroxenoid mineral rhodonite. Materials Research Bulletin, 15, 73–79.

Angel, R.J., Price, G.D., and Putnis, A. (1984) A mechanism for pyroxene-pyroxenoid and pyroxenoid-pyroxenoid transformations. Physics and Chemistry of Minerals, 10, 236–243.

Brown, P.E., Essene, E.J., and Peacor, D.R. (1980) Phase relations inferred from field data for Mn pyroxenes and pyroxenoids. Contributions to Mineralogy and Petrology, 74, 417–425.

Burnham, C.W. (1971) The crystal structure of pyroxferroite from Mare Tranquillitatis. Proceedings of the Second Lunar Science Conference, 1, 47–57.

Cameron, M., and Papike, J.J. (1981) Structural and chemical variations in pyroxenes. American Mineralogist, 66, 1–50.

Czank, M., and Liebau, F. (1980) Periodicity faults in chain silicates: A new type of planar lattice fault observed with high resolution electron microscopy. Physics and Chemistry of Minerals, 6, 85–94.

Czank, M., and Simons, B. (1983) High resolution electron microscopic studies on ferrosilite III. Physics and Chemistry of Minerals, 9, 229–234.

Finger, L.W., and Hazen, R.M. (1978) Refined occupancy factors for synthetic Mn-Mg pyroxmangite and rhodonite. Carnegie Institution of Washington Year Book 77, 850–853.

Freed, R.L., and Peacor, D.R. (1967) Refinement of the crystal structure of johannsenite. American Mineralogist, 52, 709–720.

Ghose, S., and Wan, C. (1975) Crystal structures of $CaCoSi_2O_6$ and $CaNiSi_2O_6$: Crystal chemical relations in C2/c pyroxenes (abs.). EOS, 56, 1076.

Hazen, R.M., and Wones, D.R. (1972) The effect of cation substitutions on the physical properties of trioctahedral micas. American Mineralogist, 57, 103–129.

——— (1978) Predicted and observed compositional limits of trioctahedral micas. American Mineralogist, 63, 885–892.

Hill, R.J., and Gibbs, G.V. (1979) Variation in d(T–O), d(T···T) and <T–O–T in silica and silicate minerals, phosphates, and aluminates. Acta Crystallographica, B35, 25–30.

Ito, J. (1972) Rhodonite-pyroxmangite peritectic along the join $MnSiO_3$-$MgSiO_3$ in air. American Mineralogist, 57, 865–876.

Koto, K., Morimoto, N., and Narita, H. (1976) Crystallographic relationships of the pyroxenes and pyroxenoids. Journal of the Japanese Association of Mineralogy, Petrology, and Economic Geology, 71, 248–254.

Liebau, F. (1962) Die Systematik der Silikate, Naturwissenschaften, 49, 481–491.

Maresch, W.V., and Mottana, A. (1976) The pyroxmangite-rhodonite transformation for the $MnSiO_3$ composition. Contributions to Mineralogy and Petrology, 55, 69–79.

Morimoto, N., Koto, K., and Shinohara, T. (1966) Oriented transformation, johannsenite to bustamite. Mineralogical Journal, 5, 44–64.

Murakami, T., and Takéuchi, Y. (1979) Structure of synthetic rhodonite, $Mn_{0.685}Mg_{0.315}SiO_3$, and compositional transformations in pyroxenoids. Mineralogical Journal, 9, 186–304.

Narita, H., Koto, K., and Morimoto, N. (1977) The crystal structures of $MnSiO_3$ polymorphs (rhodonite- and pyroxmangite-type). Mineralogical Journal, 8, 329–342.

Ohashi, Y., and Burnham, C.W. (1973) Clinopyroxene lattice deformations: The roles of chemical substitution and temperature. American Mineralogist, 58, 843–849.

Ohashi, Y., and Finger, L.W. (1975) Pyroxenoids: A comparison of refined structures of rhodonite and pyroxmangite. Carnegie Institution of Washington Year Book 74, 564–569.

——— (1978) The role of octahedral cations in pyroxenoid crystal chemistry. I. Bustamite, wollastonite, and the pectolite-schizolite-serandite series. American Mineralogist, 63, 274–288.

Ohashi, Y., Burnham, C.W., and Finger, L.W. (1975) The effect of Ca-Fe substitution on the clinopyroxene crystal structure. American Mineralogist, 60, 423–434.

Peacor, D.R., Essene, E.J., Brown, P.E., and Winter, G.A. (1978) The crystal chemistry and petrogenesis of a magnesian rhodonite. American Mineralogist, 63, 1137–1142.

Pinckney, L.R., and Burnham, C.W. (1988) High-temperature crystal structure of pyroxmangite. American Mineralogist, 73, 809–817.

Prewitt, C.T., and Peacor, D.R. (1964) Crystal chemistry of the pyroxenes and pyroxenoids. American Mineralogist, 49, 1527–1542.

Ribbe, P.H., and Prunier, A.R., Jr. (1977) Stereochemical systematics of ordered C2/c silicate pyroxenes. American Mineralogist, 62, 710–720.

Ried, H., and Korekawa, M. (1980) Transmission electron microscopy of synthetic and natural fünferketten and siebenerketten pyroxenoids. Physics and Chemistry of Minerals, 5, 351–365.

Robinson, K., Gibbs, G.V., and Ribbe, P.H. (1971) Quadratic elongation: A quantitative measure of distortion in coordination polyhedra. Science, 172, 567–570.

Takéuchi, Y. (1977) Designation of cation sites in pyroxenoids. Mineralogical Journal, 8, 431–438.

Thompson, J.B., Jr. (1978) Biopyriboles and polysomatic series. American Mineralogist, 63, 239–249.

Veblen, D.R. (1985) TEM study of a pyroxene-to-pyroxenoid reaction. American Mineralogist, 70, 885–901.

Weber, H.-P. (1983) Ferrosilite III, the high-temperature polymorph of $FeSiO_3$. Acta Crystallographica, C39, 1–3.

Manuscript received July 15, 1986
Manuscript accepted March 4, 1988

Table A1. Unit-cell data for pyroxmangite and rhodonite

Pyroxmangite	Nar-P	Aj-P	OF-P	FH-P	Roth-P	CWB-P
a (Å)	9.770(3)	9.712(2)	9.690(2)	9.585(1)	9.519(5)	9.635(1)
b (Å)	10.495(4)	10.536(2)	10.505(3)	10.359(1)	10.280(5)	10.431(1)
c (Å)	17.455(6)	17.438(3)	17.391(3)	17.247(2)	17.125(9)	17.381(2)
α (deg)	111.8(1)	112.15(1)	112.17(2)	112.335(3)	112.35(5)	112.23(2)
β (deg)	102.3(1)	102.88(1)	102.85(1)	102.497(7)	102.33(5)	103.56(2)
γ (deg)	82.9(1)	82.95(2)	82.93(2)	83.097(7)	82.96(5)	82.45(2)
V_{cell}(Å^3)	1625(1)	1609.8(.05)	1596.7(6)	1545.1(2)	1513(1)	1570.6(4)

Rhodonite	Nar-R	OF-R	Peac-R	MT-R	FH-R
a (Å)	9.759(4)	9.758(1)	9.797(3)	9.682(3)	9.649(2)
b (Å)	10.523(6)	10.499(1)	10.497(3)	10.435(4)	10.389(3)
c (Å)	12.235(4)	12.205(1)	12.185(4)	12.149(3)	12.108(3)
α (deg)	108.6(1)	108.58(1)	108.55(4)	108.55(3)	108.65(2)
β (deg)	102.7(1)	102.92(1)	103.02(4)	102.46(4)	102.32(2)
γ (deg)	82.7(1)	82.52(1)	82.49(4)	82.88(3)	82.95(2)
V_{cell}(Å^3)	1160(1)	1152.9(2)	1155.1(7)	1141.3(7)	1121.6(5)

Table A2. Bond distances for pyroxmangite and rhodonite

Bond	Nar-P	Aj-P	OF-P	FH-P	Roth-P	CWB-P
		I. Pyroxmangite M-O distances (Å)				
M1-OA1	2.141	2.156	2.149	2.128	2.083	2.127
-OA1	2.336	2.321	2.312	2.290	2.259	2.305
-OA2	2.277	2.623	2.247	2.202	2.181	2.233
-OA6	2.262	2.276	2.255	2.227	2.182	2.274
-OA7	2.161	2.142	2.136	2.098	2.069	2.074
-OA8	2.163	2.164	2.144	2.100	2.062	2.098
Mean	2.223(9)	2.220(1)	2.207(4)	2.174(3)	2.139	2.185(2)
M2-OA2	2.175	2.170	2.158	2.119	2.097	2.145
-OA6	2.320	2.283	2.276	2.238	2.225	2.212
-OA3	2.342	2.330	2.313	2.260	2.220	2.220
-OA5	2.209	2.216	2.195	2.157	2.158	2.208
-OB3	2.154	2.140	2.123	2.077	2.071	2.093
-OB4	2.118	2.107	2.089	2.035	2.009	2.078
Mean	2.220(9)	2.208(1)	2.192(4)	2.148(4)	2.130	2.159(2)
M3-OA3	2.190	2.199	2.177	2.152	2.129	2.174
-OA4	2.191	2.182	2.183	2.148	2.111	2.171
-OA4	2.384	2.380	2.351	2.339	2.359	2.269
-OA5	2.258	2.255	2.240	2.209	2.174	2.156
-OB2	2.190	2.173	2.166	2.119	2.080	2.143
-OB5	2.118	2.089	2.084	2.045	2.004	2.056
Mean	2.222(9)	2.213(1)	2.200(4)	2.169(4)	2.143	2.162(2)
M4-OA3	2.268	2.242	2.234	2.210	2.165	2.224
-OA6	2.152	2.151	2.124	2.087	2.058	2.093
-OA8	2.334	2.322	2.338	2.298	2.245	2.335
-OB1	2.245	2.216	2.209	2.165	2.140	2.172
-OB2	2.079	2.067	2.068	2.032	2.007	2.065
-OC6	2.257	2.255	2.230	2.189	2.151	2.191
Mean	2.223(9)	2.209(1)	2.201(4)	2.164(3)	2.128	2.180(2)

Table A2 (Continued)

Bond	Nar-P	Aj-P	OF-P	FH-P	Roth-P	CWB-P
M5-OA5	2.206	2.189	2.187	2.176	2.123	2.217
-OA4	2.125	2.137	2.137	1.118	2.080	2.163
-OB4	2.109	2.100	2.103	2.099	2.081	2.147
-OB5	2.122	2.134	2.141	2.151	2.130	2.191
-OC3	2.774	2.765	2.739	2.645	2.659	2.683
-OC4	2.528	2.513	2.508	2.426	2.361	2.492
-OC2	2.927	2.901	2.900	2.881	2.850	2.839
Mean(7)	2.399(9)	2.392(1)	2.387(4)	2.356(4)	2.326	2.390(2)
Mean(6)	2.311(9)	2.307(1)	2.300(4)	2.269(4)	2.239	2.316(2)
M6-OA1	2.146	2.121	2.096	2.059	2.044	2.058
-OA8	2.248	2.214	2.207	2.165	2.140	2.217
-OB1	2.041	2.053	2.027	1.989	1.978	2.012
-OB6	2.006	1.987	1.958	1.922	1.906	1.922
-OC7	2.396	2.384	2.371	2.268	2.227	2.382
-OA7	2.796	2.807	2.761	2.620	2.566	2.902
Mean(6)	2.272(9)	2.261(1)	2.237(4)	2.170(4)	2.143	2.249(2)
Mean(5)	2.167(9)	2.152(1)	2.132(4)	2.081(4)	2.059	2.118(3)
M7-OA2	2.234	2.237	2.226	2.188	2.149	2.237
-OA7	2.168	2.134	2.147	2.142	2.088	2.173
-OB3	2.071	2.079	2.084	2.070	2.031	2.160
-OB6	2.101	2.116	2.122	2.125	2.090	2.182
-OC1	2.579	2.581	2.569	2.586	2.524	2.516
-OC5	2.549	2.529	2.490	2.378	2.311	2.466
-OC2	2.960	2.957	2.920	2.844	2.865	2.864
Mean(7)	2.380(9)	2.376(1)	2.365(4)	2.333(4)	2.294	2.371(2)
Mean(6)	2.284(9)	2.280(1)	2.272(4)	2.248(4)	2.199	2.289(2)
	II. Pyroxmangite Si-O distances (Å)					
Si1-OA1	1.641	1.621	1.635	1.625	1.639	1.629
-OB1	1.590	1.585	1.592	1.585	1.588	1.615
-OC1	1.642	1.637	1.659	1.652	1.661	1.649
-OC7	1.644	1.655	1.636	1.652	1.643	1.649
Mean	1.629(9)	1.624(1)	1.631(4)	1.628(4)	1.633	1.636(3)
Si2-OA2	1.625	1.613	1.619	1.625	1.625	1.611
-OB2	1.605	1.589	1.590	1.588	1.594	1.609
-OC2	1.625	1.643	1.636	1.632	1.625	1.636
-OC1	1.667	1.677	1.662	1.658	1.658	1.664
Mean	1.631(9)	1.630(1)	1.627(4)	1.626(4)	1.625	1.630(3)
Si3-OA3	1.616	1.605	1.621	1.613	1.636	1.616
-OB3	1.598	1.596	1.598	1.594	1.587	1.585
-OC3	1.644	1.630	1.629	1.621	1.607	1.630
-OC2	1.673	1.651	1.651	1.650	1.650	1.661
Mean	1.633(9)	1.620(1)	1.625(4)	1.620(4)	1.620	1.623(3)
Si4-OA4	1.629	1.613	1.608	1.607	1.613	1.601
-OB4	1.614	1.594	1.601	1.596	1.594	1.594
-OC4	1.638	1.643	1.651	1.644	1.644	1.637
-OC3	1.633	1.638	1.637	1.637	1.638	1.642
Mean	1.629(9)	1.622(1)	1.625(4)	1.621(4)	1.622	1.619(3)
Si5-OA5	1.622	1.608	1.613	1.606	1.626	1.605
-OB5	1.580	1.595	1.597	1.585	1.593	1.592
-OC5	1.649	1.640	1.650	1.639	1.637	1.628
-OC4	1.652	1.652	1.639	1.650	1.646	1.639
Mean	1.626(9)	1.624(1)	1.625(4)	1.620(4)	1.625	1.616(3)
Si6-OA6	1.617	1.602	1.618	1.608	1.615	1.608
-OB6	1.596	1.585	1.595	1.588	1.589	1.598
-OC6	1.624	1.642	1.649	1.639	1.643	1.651
-OC5	1.630	1.629	1.627	1.638	1.641	1.632
Mean	1.617(9)	1.615(1)	1.622(4)	1.618(4)	1.622	1.622(3)
Si7-OA7	1.602	1.585	1.598	1.591	1.600	1.569
-OA8	1.598	1.607	1.608	1.603	1.606	1.612
-OC7	1.664	1.650	1.660	1.649	1.655	1.646
-OC6	1.663	1.643	1.651	1.658	1.654	1.654
Mean	1.632(9)	1.621(1)	1.629(4)	1.625(4)	1.628	1.620(3)

Bond	Nar-R	OF-R	Peac-R	MT-R	FH-R
	III. Rhodonite M-O distances (Å)				
M1-OA1	2.170	2.170	2.182	2.166	2.152
-OA1	2.331	2.327	2.333	2.306	2.302
-OA2	2.263	2.265	2.268	2.257	2.243
-OA4	2.253	2.256	2.253	2.230	2.214
-OA5	2.155	2.134	2.139	2.130	2.113
-OA6	2.139	2.129	2.137	2.109	2.093
Mean	2.219(7)	2.213(4)	2.219(3)	2.200(3)	2.186(3)
M2-OA2	2.229	2.215	2.213	2.200	2.187
-OA4	2.373	2.361	2.353	2.369	2.361
-OA3	2.236	2.243	2.242	2.224	2.216
-OA3	2.329	2.292	2.280	2.288	2.273
-OB2	2.143	2.147	2.150	2.135	2.119
-OB3	2.140	2.112	2.089	2.105	2.085
Mean	2.242(7)	2.228(4)	2.221(4)	2.220(3)	2.207(3)
M3-OA3	2.246	2.249	2.253	2.246	2.237
-OB2	2.102	2.099	2.104	2.068	2.060
-OA4	2.137	2.122	2.118	2.102	2.083
-OA6	2.366	2.274	2.392	2.342	2.328
-OB1	2.216	2.217	2.198	2.200	2.189
-OC4	2.273	2.243	2.234	2.220	2.204
Mean	2.223(7)	2.217(4)	2.217(3)	2.196(3)	2.184(3)
M4-OA1	2.140	2.108	2.090	2.084	2.069
-OA6	2.246	2.228	2.195	2.219	2.200
-OB1	2.069	2.042	2.026	2.013	2.002
-OB4	2.004	1.972	1.954	1.958	1.943
-OC5	2.367	2.348	2.334	2.297	2.273
-OA5	2.778	2.793	2.770	2.672	2.627
Mean(6)	2.267(7)	2.248(4)	2.228(3)	2.207(3)	2.186(3)
Mean(5)	2.165(7)	2.140(4)	2.207(3)	2.114(3)	2.098(3)
M5-OA2	2.192	2.222	2.270	2.172	2.161
-OA5	2.150	2.180	2.224	2.148	2.149
-OB3	2.099	2.154	2.236	2.109	2.111
-OB4	2.113	2.159	2.239	2.125	2.128
-OC1	2.685	2.652	2.631	2.710	2.715
-OC3	2.715	2.619	2.532	2.573	2.529
-OC2	2.828	2.782	2.708	2.766	2.739
Mean(7)	2.397(7)	2.395(4)	2.406(4)	2.372(3)	2.362(3)
Mean(6)	2.325(7)	2.331(4)	2.356(4)	2.306(3)	2.299(3)

Table A2 (Continued)

Bond	Nar-R	OF-R	Peac-R	MT-R	FH-R
	IV. Rhodonite Si-O distances (Å)				
Si1-OA1	1.622	1.627	1.629	1.629	1.627
-OB1	1.588	1.582	1.590	1.590	1.587
-OC1	1.639	1.653	1.657	1.642	1.647
-OC5	1.642	1.643	1.642	1.649	1.644
Mean	1.623(7)	1.626(4)	1.630(3)	1.628(3)	1.626(3)
Si2-AO2	1.623	1.614	1.613	1.618	1.622
-OB2	1.600	1.597	1.598	1.591	1.594
-OC2	1.627	1.637	1.638	1.624	1.622
-OC1	1.657	1.649	1.655	1.652	1.641
Mean	1.627(7)	1.624(4)	1.626(3)	1.621(3)	1.619(3)
Si3-OA3	1.623	1.610	1.613	1.614	1.614
-OB3	1.596	1.595	1.591	1.590	1.591
-OC3	1.617	1.626	1.627	1.621	1.624
-OC2	1.645	1.645	1.657	1.646	1.641
Mean	1.620(7)	1.619(4)	1.622(3)	1.618(4)	1.618(4)
Si4-OA4	1.617	1.603	1.617	1.608	1.612
-OB4	1.596	1.602	1.587	1.597	1.592
-OC4	1.639	1.648	1.644	1.641	1.644
-OC3	1.616	1.624	1.632	1.627	1.625
Mean	1.617(7)	1.619(4)	1.620(3)	1.618(3)	1.618(3)
Si5-OA5	1.592	1.587	1.597	1.595	1.594
-OA6	1.611	1.611	1.609	1.608	1.610
-OC5	1.649	1.648	1.659	1.651	1.650
-OC4	1.638	1.647	1.660	1.653	1.652
Mean	1.623(7)	1.623(3)	1.632(3)	1.627(3)	1.627(3)

* For estimated standard deviation errors on individual bond distances, the reader is referred to the original papers. Errors on Rothbard distances are not known.

Table A3. Cation occupancies in pyroxmangite and rhodonite*

Pyroxmangites

Site	Nar-P Mn	Nar-P Mg	Aj-P Mn	Aj-P Mg	OF-P Mn	OF-P Mg	FH-P Mn	FH-P Mg	Roth-P Mn	Roth-P Mg
1										
M1	1.0	0.0	0.973	0.027(7)	0.97	0.03(1)	0.516	0.484(5)	0.04	0.96(1)
M2	1.0	0.0	0.952	0.048(7)	0.81	0.19(1)	0.351	0.649(6)	0.00	1.00(1)
M3	1.0	0.0	0.962	0.038(7)	0.83	0.17(1)	0.451	0.549(5)	0.05	0.95(1)
M4	1.0	0.0	0.967	0.033(7)	0.89	0.11(1)	0.452	0.548(5)	0.03	0.97(1)
M5	1.0	0.0	0.999	0.001(7)	0.88	0.12(1)	0.788	0.212(5)	0.30	0.70(1)
M6	1.0	0.0	0.921	0.079(7)	0.81	0.19(1)	0.253	0.747(5)	-.02	1.02(1)
M7	1.0	0.0	1.00	0.00	0.91	0.09	0.777	0.223	0.27	0.73

Rhodonites

Site	Nar-R Mn	Nar-R Mg	OF-R Mn	OF-R Mg	Peac-R Mn	Peac-R Mg	MT-R Mn	MT-R Mg	FH-R Mn	FH-R Mg
M1	1.0	0.0	0.93	0.07(1)	0.89	0.11(1)	0.696	0.304(6)	0.615	0.383(5)
M2	1.0	0.0	0.93	0.07(1)	0.86	0.14(1)	0.746	0.254(6)	0.687	0.313(5)
M3	1.0	0.0	0.91	0.09(1)	0.86	0.14(1)	0.634	0.366(6)	0.572	0.428(5)
M4	1.0	0.0	0.78	0.22(1)	0.53	0.47(1)	0.481	0.519(6)	0.350	0.650(5)
M5	1.0	0.0	0.83	0.17	0.40	0.60(ca)	0.868	0.132	0.876	0.124

*Obtained from least- squares refinement using a linear combination of Mn-Mg. Mn and Fe were grouped together, while Ca effectively increases the apparent Mg occupancy. Total composition was constrained in each refinement.

Appendixes continued on the next page

Table A4

		Nar-P	Aj-P	OF-P	FH-P	Roth-P	CWB-P
	I.	Pyroxmangite: Tetrahedral volumes Å^3 and distortions					
Si1	V	2.21	2.19	2.21	2.20	2.19	2.23
	λ	1.0037	1.0040	1.0041	1.0058	1.0065	1.0041
	σ^2	13.39	14.50	15.40	22.14	24.49	15.50
Si2	V	2.21	2.22	2.20	2.19	2.19	2.21
	λ	1.0040	1.0037	1.0039	1.0047	1.0050	1.0042
	σ^2	16.50	15.49	16.58	19.68	21.16	18.05
Si3	V	2.22	2.17	2.19	2.16	2.16	2.18
	λ	1.0040	1.0040	1.0040	1.0056	1.0066	1.0046
	σ^2	17.03	17.09	17.06	23.49	27.95	19.28
Si4	V	2.20	2.17	2.18	2.17	2.16	2.16
	λ	1.0046	1.0054	1.0056	1.0066	1.0079	1.0066
	σ^2	19.18	22.66	23.51	27.76	32.35	28.11
Si5	V	2.18	2.18	2.18	2.15	2.16	2.14
	λ	1.0087	1.0079	1.0083	1.0094	1.0102	1.0085
	σ^2	35.53	33.51	34.88	39.19	41.80	35.91
Si6	V	2.13	2.12	2.15	2.13	2.14	2.15
	λ	1.0116	1.0122	1.0127	1.0143	1.0164	1.0113
	σ^2	47.08	49.66	51.06	57.51	65.96	44.91
Si7	V	2.20	2.15	2.18	2.16	2.15	2.14
	λ	1.0110	1.0121	1.0110	1.0131	1.0156	1.0132
	σ^2	48.76	54.88	49.09	58.98	69.44	59.78
	II.	Pyroxmangite: Octahedral volumes and distortions					
M1	V	14.26	14.21	13.94	13.35	12.79	13.48
	λ	1.020	1.020	1.020	1.019	1.019	1.023
	σ^2	61.25	60.88	62.66	56.52	55.50	66.57
M2	V	14.27	14.03	13.72	12.91	12.60	13.18
	λ	1.016	1.016	1.018	1.017	1.020	1.013
	σ^2	52.56	53.53	56.31	53.79	64.90	41.86
M3	V	14.34	14.14	13.92	13.30	12.81	13.22
	λ	1.014	1.015	1.015	1.017	1.020	1.013
	σ^2	44.68	45.58	46.47	52.77	60.18	42.21
M4	V	13.67	13.41	13.24	12.61	12.05	12.82
	λ	1.048	1.049	1.050	1.048	1.044	1.053
	σ^2	163.83	168.20	170.28	163.46	150.80	178.81
M5	V(6)	12.23	12.22	12.10	11.80	11.43	11.99
	λ	1.233	1.228	1.231	1.213	1.208	1.249
	σ^2	455.02	457.28	466.99	459.04	445.49	519.05
	V(7)	18.51	18.38	18.28	17.68	17.00	18.14
M6	V(6)	13.88	12.72	13.33	12.51	12.10	13.23
	λ	1.098	1.097	1.094	1.071	1.065	1.119
	σ^2	256.97	248.32	240.57	185.92	172.11	289.23
	V(5)	7.52	7.37	7.20	6.68	6.46	7.06
M7	V(6)	14.63	14.40	14.38	13.90	13.18	14.62
	λ	1.065	1.066	1.066	1.066	1.060	1.066
	σ^2	175.83	185.58	190.18	196.72	179.03	207.76
	V(7)	18.16	18.00	17.81	17.17	16.37	18.01

Table A4 (continued)

		Nar-R	OF-R	Peac-R	MT-R	FH-R
	III.	Rhodonite: Tetrahedral volumes and distortions				
Si1	V	2.18	2.20	2.21	2.20	2.19
	λ	1.0038	1.0037	1.0038	1.0045	1.0048
	σ^2	14.51	13.96	14.74	17.48	18.88
Si2	V	2.20	2.19	2.19	2.17	2.27
	λ	1.0044	1.0044	1.0048	1.0044	1.0046
	σ^2	19.06	19.15	20.81	19.05	19.59
Si3	V	2.17	2.16	2.17	2.15	2.15
	λ	1.0049	1.0067	1.0072	1.0066	1.0068
	σ^2	20.48	28.50	30.39	28.05	28.51
Si4	V	2.14	2.15	2.15	2.14	2.14
	λ	1.0092	1.0105	1.0100	1.0113	1.0120
	σ^2	37.30	42.73	40.03	45.58	48.01
Si5	V	2.16	2.16	2.19	2.17	2.17
	λ	1.0115	1.0122	1.0131	1.0125	1.0136
	σ^2	51.59	54.84	58.99	56.35	61.19
	IV.	Rhodonite: Octahedral volumes and distortions				
M1	V	14.14	14.06	14.17	13.80	13.55
	λ	1.021	1.020	1.019	1.020	1.020
	σ^2	65.14	60.81	57.45	60.55	60.21
M2	V	14.48	14.28	14.18	14.06	13.79
	λ	1.026	1.024	1.022	1.027	1.028
	σ^2	88.80	78.37	69.35	89.32	92.28
M3	V	13.57	13.46	13.44	13.11	12.89
	λ	1.054	1.054	1.056	1.053	1.053
	σ^2	183.56	182.87	185.30	176.42	175.89
M4	V(6)	13.84	13.57	13.36	13.06	12.78
	λ	1.094	1.092	1.084	1.076	1.070
	σ^2	246.52	235.63	211.22	199.96	184.82
	V(5)	7.55	7.34	7.18	6.99	6.83
M5	V(6)	15.02	15.16	15.58	14.70	14.55
	λ	1.090	1.084	1.083	1.085	1.085
	σ^2	234.06	240.38	256.17	235.73	240.27
	V(7)	18.57	18.64	19.01	18.07	17.87

Polyhedral volumes and distortions were calculated using the computer program VOLCAL, written by L. W. Finger. The distortion parameters of mean quadratic elongation and angle variance are defined by Robinson et al (1971).

Table A5. Tetrahedral chain angles in pyroxmangite and rhodonite

Pyroxmangites:

Angle*	Nar-P	Aj-P	OF-P	FH-P	Roth-P	CWB-P
OC1-2-3	147.8	148.1	148.9	150.5	147.9	150.7
OC2-3-4	164.4	165.1	165.9	168.6	167.9	166.4
OC3-4-5	176.6	177.4	177.6	176.2	174.1	177.7
OC4-5-6	168.6	167.7	166.9	163.4	160.1	167.1
OC5-6-7	145.6	144.9	143.7	141.7	139.6	144.1
OC6-7-1	161.5	161.4	162.2	161.7	162.9	162.0
OC7-1-2	158.0	157.8	157.8	156.4	158.5	157.3

Rhodonites:

Angle	Nar-R	OF-R	Peac-R	MT-R	FH-R
OC1-2-3	154.6	156.1	158.4	156.7	157.6
OC2-3-4	177.6	177.6	174.5	176.8	175.4
OC3-4-5	150.1	147.3	145.0	146.3	145.2
OC4-5-1	160.0	160.6	161.1	160.3	160.4
OC5-1-2	154.1	153.8	153.3	153.0	152.5

* Angles formed by bridging oxygen atoms; e.g. read OC1-2-3 as the angle formed by oxygens OC1-OC2-OC3